RESEARCH ARTICLE | MARCH 10 2021

Attosecond state-resolved carrier motion in quantum materials probed by soft x-ray XANES

Bárbara Buades ; Antonio Picón ; Emma Berger ; Iker León ; Nicola Di Palo ; Seth L. Cousin; Caterina Cocchi ; Eric Pellegrin ; Javier Herrero Martin ; Samuel Mañas-Valero ; Eugenio Coronado; Thomas Danz ; Claudia Draxl ; Mitsuharu Uemoto ; Kazuhiro Yabana; Martin Schultze; Simon Wall; Michael Zürch; Jens Biegert

Appl. Phys. Rev. 8, 011408 (2021)
https://doi.org/10.1063/5.0020649

Applied Physics Reviews ARTICLE scitation.org/journal/are

Attosecond state-resolved carrier motion in quantum materials probed by soft x-ray XANES

Cite as: Appl. Phys. Rev. 8, 011408 (2021); doi: 10.1063/5.0020649
Submitted: 2 July 2020 · Accepted: 15 February 2021 ·
Published Online: 10 March 2021 · Corrected: 29 March 2021

Bárbara Buades,[1] Antonio Picón,[1,2] Emma Berger,[3,4] Iker León,[1] Nicola Di Palo,[1] Seth L. Cousin,[1] Caterina Cocchi,[5] Eric Pellegrin,[6] Javier Herrero Martin,[6] Samuel Mañas-Valero,[7] Eugenio Coronado,[7] Thomas Danz,[8] Claudia Draxl,[5] Mitsuharu Uemoto,[9] Kazuhiro Yabana,[9] Martin Schultze,[10] Simon Wall,[1] Michael Zürch,[3,4,11] and Jens Biegert[1,11,12,a)]

AFFILIATIONS

[1]ICFO-Institut de Ciencies Fotoniques, The Barcelona Institute of Science and Technology, Castelldefels (Barcelona), Spain
[2]Departamento de Química, Universidad Autónoma de Madrid, Madrid, Spain
[3] Department of Chemistry, University of California at Berkeley, Berkeley, California, USA
[4] Materials Sciences Division, Lawrence Berkeley National Laboratory, Berkeley, California, USA
[5]Institut für Physik and IRIS Adlershof, Humboldt-Universität zu Berlin, Berlin, Germany
[6]ALBA Synchrotron Light Source, Cerdanyola del Vallès, Barcelona, Spain
[7]Instituto de Ciencia Molecular (ICMol), Universitat de València, Paterna, Spain
[8]4th Physical Institute - Solids and Nanostructures, University of Göttingen, Göttingen, Germany.
[9]Center for Computational Sciences, University of Tsukuba, Tsukuba, Japan
[10]Institute of Experimental Physics, Graz University of Technology, Graz, Austria
[11]Fritz Haber Institute of the Max Planck Society, Berlin, Germany
[12]ICREA, Pg. Lluís Companys 23, Barcelona, Spain

[a)]**Author to whom correspondence should be addressed:** jens.biegert@icfo.eu

ABSTRACT

Recent developments in attosecond technology led to table-top x-ray spectroscopy in the soft x-ray range, thus uniting the element- and state-specificity of core-level x-ray absorption spectroscopy with the time resolution to follow electronic dynamics in real-time. We describe recent work in attosecond technology and investigations into materials such as Si, SiO_2, GaN, Al_2O_3, Ti, and TiO_2, enabled by the convergence of these two capabilities. We showcase the state-of-the-art on isolated attosecond soft x-ray pulses for x-ray absorption near-edge spectroscopy to observe the 3d-state dynamics of the semi-metal TiS_2 with attosecond resolution at the Ti L-edge (460 eV). We describe how the element- and state-specificity at the transition metal L-edge of the quantum material allows us to unambiguously identify how and where the optical field influences charge carriers. This precision elucidates that the Ti:3d conduction band states are efficiently photo-doped to a density of 1.9×10^{21} cm^{-3}. The light-field induces coherent motion of intra-band carriers across 38% of the first Brillouin zone. Lastly, we describe the prospects with such unambiguous real-time observation of carrier dynamics in specific bonding or anti-bonding states and speculate that such capability will bring unprecedented opportunities toward an engineered approach for designer materials with pre-defined properties and efficiency. Examples are composites of semiconductors and insulators like Si, Ge, SiO_2, GaN, BN, and quantum materials like graphene, transition metal dichalcogens, or high-Tc superconductors like NbN or LaBaCuO. Exiting are prospects to scrutinize canonical questions in multi-body physics, such as whether the electrons or lattice trigger phase transitions.

I. INTRODUCTION

Until the last decade, ultrafast soft x-ray spectroscopies were nearly exclusively available at synchrotrons, where tens- to hundreds-of-picoseconds temporal resolution was "state-of-the-art." Femto-slicing was developed to improve the time resolution to the ~150 femtoseconds range,[1,2] but at the expense of photon flux. Table-top laser-driven plasma sources are an alternative that provides incoherent emission of soft and hard x-ray bursts of radiation with temporal duration in

the sub-100 femtosecond range.[3,4] A challenge for these sources is the need for shielding from debris and the requirement for high numerical aperture x-ray optics to capture the incoherent x-ray emission. With the discovery of high-harmonic generation (HHG),[5,6] the first table-top technology became available, which yields fully coherent radiation and achieves attosecond temporal resolution. HHG suffered from the low flux and low photon energies in the extreme ultraviolet (XUV) range. These issues precluded its utility for core-level x-ray spectroscopy since the conditions to achieve element- and state-specificity could not be met. However, several breakthroughs were made during the last years to leverage the prospects of ponderomotive scaling of HHG.[7,8] Isolated attosecond soft x-ray pulses[9–12] with water-window coverage[9,13–15] are available, and the utility of attosecond technology for x-ray absorption near-edge spectroscopy (XANES)[9,16,17] and extended x-ray absorption fine structure (EXAFS)[18,19] was demonstrated. In parallel with these developments, the first self-amplified spontaneous emission (SASE) operation of an accelerator has been shown to yield x-ray radiation.[20] This achievement has led to the development of so-called "4th generation light sources" in the accelerator community, namely large-scale x-ray free electron laser facilities (XFELs), which provide unsurpassed photon flux (mostly) at hard x-ray photon energies. Due to the SASE process's inherent randomness, intensive developments are underway to achieve reproducible pulse duration and temporal synchronization. Presently, only a handful of XFELs exist worldwide, each having distinct parameters with only recently demonstrated capability to deliver sub-femtosecond pulses with good coherence and sufficiently high repetition rates.[21]

Further, performing experiments at such billion-euro-scale facilities poses its challenges. Interestingly, one can witness a convergence of technologies and investigations across table-top and large-scale facilities due to the tremendous prospects for investigation. Suffice it to say that the ability to bring sub-femtosecond, broadband x-ray sources to the table-top has enabled a new era of ultrafast science.

In our article, we will discuss the table-top technology. We will begin Sec. I with a discussion of state-of-the-art generation of attosecond pulses in the soft x-ray (SXR) regime using high-harmonic generation (HHG). We will then discuss the investigative techniques, namely XANES and EXAFS spectroscopy, enabled by the broadband nature of ultrafast HHG sources. Next follows an overview of recent works investigating the sub-cycle, nonlinear optical response in solid-state materials based on absorption spectroscopy. In Sec. II, we discuss the state-of-the-art method that unites isolated attosecond pulse resolution with core-level XANES. We present a case study in which we use attosecond XANES to investigate the quantum material titanium disulfide (TiS_2). This experiment is the first investigation of a semi-metallic[22–24] transition metal dichalcogen (TMDC) with an attosecond soft x-ray (SXR) probe at the Ti $L_{2,3}$ edge. This section intends to showcase what is currently possible with attosecond XANES in the water-window SXR regime to stimulate interdisciplinary collaborations between the solid-state, materials, ultrafast x-ray, and attoscience communities. The realization of such collaborations will guide the development of attosecond table-top x-ray sources, further x-ray spectroscopy theoretical methods to better model complicated material systems, and advance our understanding of complex multi-component quantum materials of relevance to address today's problems.

A. Attosecond high harmonic generation sources in the soft x-ray regime

Key to the development of table-top x-ray sources has been the advancement of HHG,[25] a process by which visible and infrared (IR) laser photons are coherently energy up-converted to wavelengths spanning the XUV and SXR regimes. Briefly, optical light is focused into a gas medium where valence electrons are ionized as the driving pulse's electric field reaches its maximum. Each newly freed electron is accelerated away from its parent ion, picking up kinetic energy as it travels along a negative gradient potential energy surface. When the oscillating electric field eventually reverses sign, the electron reverses its direction and recombines with its parent ion, resulting in a release of the excess kinetic energy it picked up from the laser field as a burst of x-rays. Because the HHG process is fully coherent and preserves the driving laser's properties, the resulting x-rays exhibit extraordinary spatio-temporal coherence and cover broadband spectral ranges with down to sub-100-attosecond temporal durations.[12] While HHG performed with widely used Ti:Sapphire 800-nm driving pulses has been a highly successful method for producing femtosecond and sub-femtosecond XUV pulses up to 120 eV, the last decade has seen a tremendous advancement in source development, enabling the generation of attosecond x-ray pulses extending well into the SXR regime.[9,14] Here, we discuss these advancements by highlighting the tunable parameters of the HHG process.

For one, the maximum possible energy of up-converted photons is given by

$$E_{cutoff} = I_p + 3.17U_p \propto I_L\lambda_L^2, \quad (1)$$

where I_p is the ionization potential of the gas target, almost always chosen to be a noble gas, and U_p is the quiver energy that scales with the intensity and square of the wavelength of the driving laser.[26] In initial works, the approach to increase E_{cutoff} simply increased the intensity of the optical driver, which was often done by shortening its duration to the near single-cycle limit.[25] However, this method proves to be limited, as plasma effects beyond the tunnel ionization regime severely limit the effective generation of high harmonic emission.

Given Eq. (1), an alternative approach, first demonstrated by Shan *et al.*,[27] is to increase the optical pulse's wavelength, thereby increasing the electron's excursion distance in the continuum to acquire higher recollisional energy upon recombination.[27] It is now standard practice for HHG setups to use parametric amplification[8,19,28–32] to down-convert 800-nm photons to wavelengths between 1.3 and 3 μm. However, the wavelength cannot be increased indefinitely to scale HHG due to dispersion of the continuum electron wavepacket, since this reduces the probability of recombination as λ^{-a}, where $5 < a < 6$.[26,33–35] With carefully tuned phase matching conditions,[36] i.e., by balancing the choice of driving wavelength, intensity, and HHG medium, HHG sources can reach wavelengths spanning the XUV to the SXR regimes [Figs. 1(a) and (b)]. Based on this concept, the first sources to reach the SXR water window with the carbon K-shell edge at 284 eV were based on 1-kHz Ti:Sapphire laser amplifier systems, which pumped optical parametric amplifiers (OPAs) at 1.5 μm[37] producing 20 ph/eV/s at 284 eV,[13] OPAs at 1.3 μm[38] with 10^7 ph/s/1% with cutoff at 300 eV, and a 1-kHz Ti:Sapphire-pumped OPA at 1.85 μm, which produces 1.9×10^7 ph/s/1% at 300 eV[9] with cutoff at

450 eV. Common to all of these systems are pump energies from the Ti;Sapphire frontend from 1 to 3 mJ. Recently, further upscaling of the Ti:Sapphire pulse energy has led to a much improved SXR photon flux. For instance, pumping a 2.1-μm[37] OPA with 19.5-mJ, 20-fs pulses from a 1-kHz Ti:Sapphire system yielded 10^9 ph/s/1% bandwidth[19] in the SXR water window.

Further increasing pulse energy at a lower repetition rate of 100 Hz, a 1.85-μm OPA produced 40-mJ, 40-fs pulses and a SXR flux of 8×10^6 ph/s integrated across entire water window.[32] Most recently, Fu *et al.*, demonstrated 3.5-nJ energy harmonics in the SXR water window from a 10-Hz, 100-mJ OPA with wavelength of 1.2–2.4 μm.[39] While there are currently various laser implementations for SXR generation,[15,40–42] the demonstrated SXR pulse energy scaling provides a route toward single-shot SXR spectroscopy and ultrafast SXR imaging by scaling the laser technology. Another essential building block in establishing attosecond spectroscopy and imaging is the capacity to measure the time-structure of the generated SXR radiation. The consequentially broader bandwidth of an attosecond pulse in the SXR water window in combination with the dramatically lower absorption cross section, and the fact that several shells contribute to photo-emission, present significant obstacles for photoelectron spectroscopies and to attosecond streaking, which relies on the unambiguous mapping of electron spectra to the attosecond pulse spectrum.[11] To circumvent such issues, photonic streaking was employed by Silva *et al.*[10] to demonstrate single isolated attosecond pulse generation in the SXR water window at 300 eV. Shortly afterward, several measurements were published, which are nevertheless based on attosecond streaking and the measurement of photoelectrons.[12,43] Despite such complications for attosecond pulse characterization, the broad bandwidth of attosecond SXR pulses are a decisive advantage for absorption spectroscopy of multi-component material systems. Simultaneously, access to the multiple component absorption edges allows disentangling lattice, charge, and spin dynamics[44] of all the material's elemental components at once. The SXR regime is especially vital for such investigations, as compared to the XUV, since elemental edges overlap less and the correspondingly high photon energies allow access to K- and L-edges of many first-row transition metals and common material constituents, like S, C, N, and O. Attosecond SXR radiation are thus ideal tools for organic chemists, biochemists, materials scientists, and solid-state physicists alike[45] since investigations of composite materials, quantum materials, adsorbates, organic electronics, twisted bilayer graphene,[46–48] high-temperature superconductors,[49] metal-organic frameworks,[50,51] carbon nanomaterials,[52,53] NV-diamond centers,[54,55] and TMDCs[22,56] will be possible.

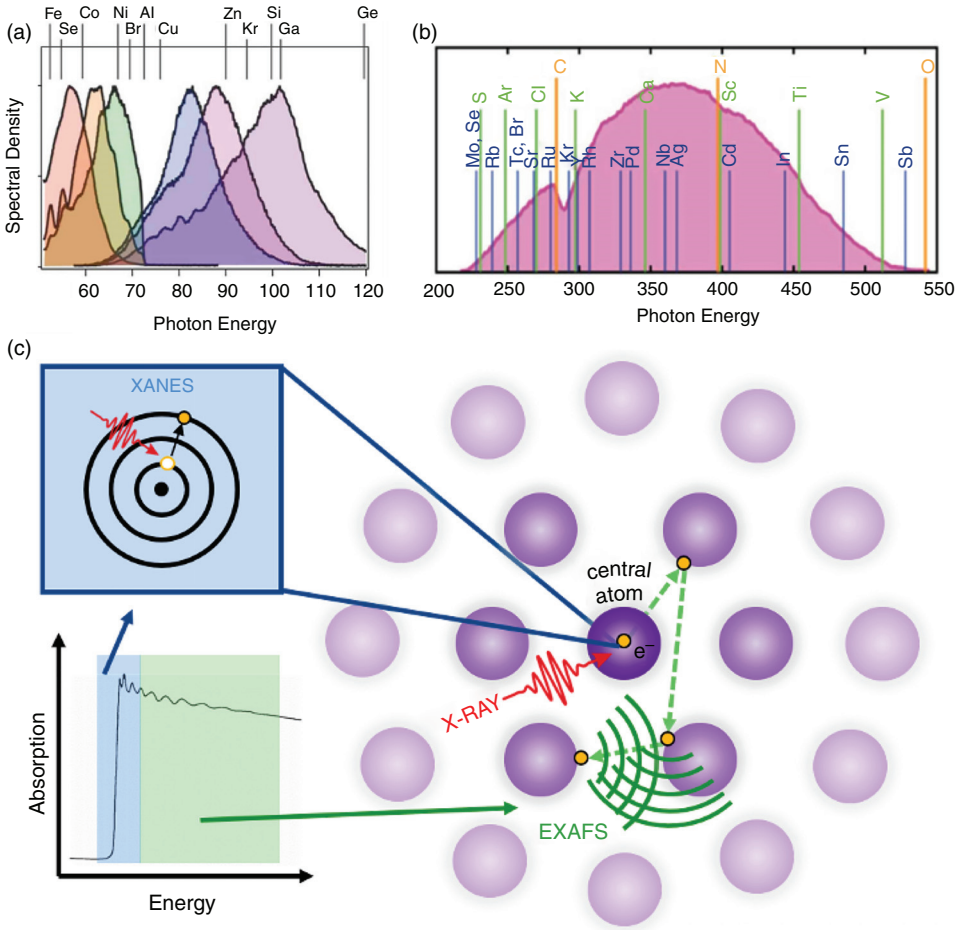

FIG. 1. Output energies of HHG-based attosecond sources and schematic of XAFS measurements. (a) Representative isolated attosecond pulse spectra generated with an 800-nm single-cycle driver pulse covering relevant absorption edges of the XUV region. Reprinted with permission from H. Timmers *et al.*, Optica 3, 707 (2016).[113] Copyright 2016 Author(s), licensed under a Creative Commons Attribution 4.0 Unported License. (b) A representative spectrum of an isolated attosecond pulse covering over 300 eV in the SXR regime generated with a single-cycle 1800-nm driver pulse. Multiple element edges are covered with K-edges, L-edges, and M-edges in orange, green, and blue, respectively. Reprinted with permission from B. Buades et al., Optica 5, 502 (2018).[18] Copyright 2018 Author(s), licensed under a Creative Commons Attribution 4.0 Unported License. (c) XANES measures unoccupied valence states (VS) using a core-electron excited by a high energy SXR photon and is, therefore, energetically relevant around absorption edges. In time-resolved XANES, an optical pulse typically first triggers an out-of-equilibrium dynamic in the valence states. EXAFS spectroscopy instead probes a larger energy window above the edge where modulations in the absorption spectrum stem from photoelectrons with enough excess energy to scatter multiple times and auto-interfere with itself. Data for absorption plot taken from Ref. 57.

X-ray absorption spectroscopy (XAS) can be easily implemented with a table-top SXR source since it directly leverages the extreme bandwidth of the attosecond pulse. The absorption of light by a sample is directly related to the imaginary part of its dielectric function and XAS is a sensitive probe of element-specific electronic structure when the incident light is resonant with an atomic edge, and if that transition is unique. These conditions are fulfilled at high photon energies, which level core transitions, thus avoiding multiplet effects and excessive photoionization. XAS methods can be further divided into XANES and EXAFS, where the difference lies in the spectral region around the absorption edge probed[18,57] [Fig. 1(c)]. Without an exact division of energy ranges, XANES roughly covers the region from the edge onset to about 50 eV above, such that absorption is dominated by resonant transitions from occupied core states to unoccupied valence states. In this regime, information about an atom's density of states, site symmetry, oxidation state, and coordination number can be obtained since the photoelectron's mean free path is on the order of the first-coordination shell. On the other hand, EXAFS is characterized by high-energy photoelectrons that travel far enough to encounter neighboring atoms. The existing autointerference between the different scattering pathways of a photoelectron will modulate its scattering cross-section, resulting in undulations of the absorption in the EXAFS regime, which can be processed by a Fourier analysis to provide information about lattice spacings and symmetry.

Key to both of these x-ray absorption fine structure (XAFS) is the ability to resolve subtle features in the absorption spectrum, which necessitates high-brightness, stable x-ray sources. For this reason, the development of synchrotron sources was instrumental to the viability of XAFS techniques. With the shortening of pulse durations and the advancement of timing schemes, time-resolved XAFS has become a popular method for investigating nonequilibrium electronic structure dynamics. Here, the >30 picosecond x-ray pulses from electron storage rings can be shortened to hundreds-of-femtoseconds with "femtoslicing" techniques. However, even these pulse durations are too long to resolve electron wavepackets that dephase with a characteristic timescale of femtoseconds.[1] On the other hand, XFELs can offer tens-of-femtosecond pulse durations but tend to be quite narrowband and spectrally unstable. For XFELs, stability, longitudinal coherence, and synchronization are significant challenges that render time-resolved fine-structure studies challenging at the present time.

Attosecond transient absorption spectroscopy (ATAS) is therefore ideally suited to exploit the prospects of time-resolved XAFS techniques to the sub-femtosecond timescales on which electron motion typically occurs. Furthermore, the broadband nature of HHG-based x-ray sources capable of covering hundreds of eV in the SXR regime allows for the simultaneous acquisition of XANES and EXAFS in a single shot with $\Delta E/E \approx 1/1000$ spectral resolution. Our group recently demonstrated combined static XAFS spectra covering over 300 eV around the Carbon K-edge in graphite, thus paving the way for attosecond, time-resolved XAFS studies.[18] Indeed, the ultrashort pulse durations offered by HHG sources and their broadband spectral characteristics will be indispensable in extending the toolbox for next-generation ultrafast science.

B. Attosecond spectroscopy: The sub-cycle optoelectronic response in solids

We now turn our discussion to the science that has been enabled by table-top attosecond x-ray spectroscopy, with a specific focus on ATAS applied to solid-state systems. For a more specified discussion on ultrafast gas-phase dynamics, we refer the reader to recent excellent reviews in Refs. 58 and 59. A series of landmark works have focused on questions related to the speed and mechanisms with which optical pulses affect material properties, with motivations driven largely by the prospects of light-wave electronics controlled at petahertz (PHz) frequencies. With single-cycle visible light pulses having few-femtosecond pulse durations, attosecond probing pulses are necessary. Further, the elemental-specificity and separation in energy-scale between the optical and XUV pulses have been invaluable to interpreting results.

Initial optical pump–XUV probe experiments were performed on SiO_2 and pure Si in the strong-field excitation regime (10^{12} W cm^{-2}). These experiments leveraged near-critical electric fields of 2.5 V/Å and sub-bandgap pulse energies, conditions under which nonlinear effects are expected to play a leading role. Indeed, reversible oscillations occurring only during the time-overlap of the pump and probe pulses at twice the pump frequency (2ω) and step-like excitation behavior following the optical pulse time-trace were observed, respectively.[16,60] In another experiment, on GaN, which is a 3.35 eV bandgap semiconductor, weak-field excitation yielded photo-excited 3ω dipole oscillations, thus showing PHz field control of carrier dynamics via a three-photon absorption process.[61] The wide bandgap insulator Al_2O_3 doped with Cr ions was subsequently studied in a similar experiment. It was shown that multi-PHz frequency manipulation was possible via interference of multiphoton processes with frequency tunability offered by choosing the identity of the chemical dopant.[62]

While the experiments mentioned above highlight optical control of semiconductors and dielectrics in the strong field regimes, Lucchini *et al.* sought to understand the competition between intra- and inter-band effects at intermediate field strengths.[63] In this mixed regime, the optoelectronic response should be described by a hybrid of the strong- and weak-field extrema: in the weak- (strong-) field limit, inter- (intra) band transitions should dominate with the pump light behaving like a photon (field). Here a 5-fs carrier-envelope-phase (CEP) stabilized below-gap IR pulse was incident on diamond, a dielectric with a 7.3 eV indirect bandgap. The XUV pulse is most commonly used to probe core-to-valence excitations, the 250 as, 42 eV probe pulse excited valence electrons to the CB continuum. The intent here was to distinguish between inter- and intra-band effects more cleanly. The resulting transient absorption spectra revealed 2ω oscillations, which were attributed to the dynamical Franz Keldysh effect (DKFE). The DKFE, in which the driving pulse's electric field bends the crystal potential enough to distort electronic wavefunctions to leak into the bandgap and make possible photon-assisted tunneling, was shown to nearly fully account for the measured signal. This experiment was recently re-performed and found to be almost instantaneous, occurring with a 49 as time constant.[64]

Building on these findings, Schlaepfer *et al.* and Volkov *et al.* used XUV-ATAS to investigate inter- and intra-band effects on the sub-cycle optoelectronic response under two different circumstances, namely, when the pump pulse is resonant with the bandgap of a semiconductor and when the material system is metallic with no bandgap at all.[65,66] In the former, it was expected that inter-band carrier dynamics would come to the forefront. Surprisingly, the observed 2ω oscillations were, again, found to be dominated by intra-band currents, though the coupling between inter- and intra-band effects was

necessary to explain the enhanced excitation of carriers across the bandgap. In the latter, ATAS was performed at the Ti $M_{2,3}$ edge in pure Ti in response to a 1×10^{12} W cm^{-2} near-infrared (NIR) pump pulse (10 fs, 1.55 eV). It was anticipated that many-body electron correlation effects (i.e., screening, collective electron motion) from the Ti 3d valence electrons would alter the relative weighting of intra- and inter-band effects in the sub-cycle optoelectronic response. Unlike in the nonzero bandgap materials where oscillatory effects were observed, the time-resolved spectrograms instead depicted a quasi-instantaneous linear response with an optical density transient following the pump laser fluence. This finding was interpreted as a breakdown of the independent-particle approximation, indeed, a consequence of correlation-driven effects. The pump pulse was found to strongly interact with conduction band electrons, causing increased electron localization and therefore strong screening, which was confirmed by theoretical calculations to manifest itself as ultrafast and linearly dependent on pump fluence.

From the results above, we highlight several important observations. For one, in less than ten years, the realization of state-of-the-art ATAS beamlines have greatly enhanced our fundamental understanding of the light-matter interaction and has brought us one step closer to realizing PHz-controlled light-wave electronics. The sub-cycle optoelectronic response depends on the strength of the field, the size of the material bandgap compared to the pump pulse's photon energy, and the inherent material properties intra- and inter-band effects playing nonintuitive relative roles. The multi-variate nature of this problem, though, leaves many unanswered questions and necessitates a more precise probe of the electronic structure and its dynamics. Secondly, we note that real advance for investigations necessitates probe pulses above about 150 eV: shallow bound states, or semi-core states in the XUV, are usually dipole-allowed small binding energies that make the interpretation of measured dynamics only meaningful if multiplet effects can be factored out.

Additionally, near-valence transitions suffer from parasitic photoionization ($\sigma \propto Z^5 {\omega_{Xray}}^{-9/2}$), thus altering the final states to be probed significantly.[67] With higher-energy SXR pulses extending up to hundreds of eV, unambiguous state-selectivity can be achieved, which permits a clean interpretation of spectra.[68,69] Consequently, attosecond sources at significantly higher photon energies,[10,11,14,70] which are much harder to implement, are highly sought-after for state-selective ATAS spectroscopy, i.e., XANES and EXAFS. Lastly, we notice that the field of attoscience has barely scratched the surface in terms of the complexity of materials being studied. The prospects to bring attosecond temporal resolution together with state and element selective core-level XANES is expected to allow a precise investigation of multi-body and correlation effects, which preclude our current understanding of many interesting phenomena in material science, ranging from Mott transitions to exotic new phases in composite quantum materials. From an application point of view, simple thin-films, wafers, and foils (i.e., SiO_2, Si, Ti, etc.) have been the topics of most ATAS works for several reasons: (1) A transmission geometry necessitates smooth surface, thin-film samples, and only a handful of commercially available samples meeting these requirements exist, with few to none having significantly novel emergent properties. (2) Except for the lightest elements, most elements do not have core-states in the XUV regime, which has previously been limited to ATAS. 3) Solid-state attoscience is an entirely new field requiring expertise in ultrafast photonics and custom instrumentation because there may exist a disconnect between the those that develop the photonic means and the materials science or synthetic chemistry communities that make interesting materials.

Moreover, most theoretical tools in solid-state physics have been developed to predict static electronic structure. Here, entirely new developments are needed to describe the nonlinear interactions arising from the pump and probe photons, with the additional challenge being to describe the multi-body state of correlated quantum materials. Nevertheless, with the elemental-specificity x-rays can offer, the study of dynamics in more technologically relevant, multi-component materials of interest to the broader scientific community is only limited by the energies accessible to HHG x-ray sources and the ability to interpret the information contained in the absorption spectrum to extract electronic, spin, and lattice information. Considering these prospects, the recent development of attosecond SXR-HHG and spectroscopies such as XANES is truly exciting.

In what follows, we will present a case study that unites all the discussed requirements for the first time. This discussion on attosecond XANES shows how state and element selectivity is achieved and how it is used to extract the ultrafast, sub-cycle electronic occupation of specific electronic states inside the semi-metallic TMDC TiS_2. This represents the first attosecond state-resolved spectroscopy measurement of carrier-band dynamics in a TMDC at the Ti $L_{2,3}$ edge and a novel, previously unexplored, perspective on the ultrafast, sub-cycle optoelectronic dynamics that ensue in a semi-metal system in the weak field regime.

II. A CASE STUDY: SOFT X-RAY ATTOSECOND XANES TO INVESTIGATE THE WEAK-FIELD OPTOELECTRONIC RESPONSE IN THE TMDC SEMI-METAL TiS_2

The exquisite electronic and optical properties of TMDCs stem from their partially filled d-orbitals resulting in complex phase diagrams and giving rise to correlated carrier dynamics that could be exploited for revolutionary new devices[71,72] in information processing, energy harvesting, or high energy density storage.[22,23,73,74] TMDCs have been unexplored in ATAS because of the difficulties of disentangling the involvement of electronic states dependent on the material's elemental constituents and the out-of-equilibrium response of carriers of the complex energetic landscape of valence and conduction band states. To further understand the behavior of these materials in optical control fields and leverage their properties for future light-field-driven devices, it is required to resolve the microscopic response of particular orbitals on the sub-optical-cycle timescale, which requires attosecond-duration and state-selective probes[76–78] for XANES. Similarly, ultrafast measurements of electron and hole dynamics may elucidate the exact pathways of charge transport, thus permitting the discrimination of carrier scattering mechanisms and energy dissipation pathways.

The chosen material, TiS_2, exhibits attractive structural and electronic properties because of its semi-metal character; e.g., it has extremely high electron and ion mobility, and its electronic and optical properties are reminiscent of its 2D isomorph.[78,79] The properties of TiS_2 arise from a tri-layered structure, shown in Fig. 2(a), which consists of hexagonal sheets of cationic $Ti^{4+}(3d^0)$ atoms sandwiched between sheets of S atoms. The atoms within the tri-layers (S-Ti-S) are covalently bonded while the tri-layers are coupled by Van der Waals

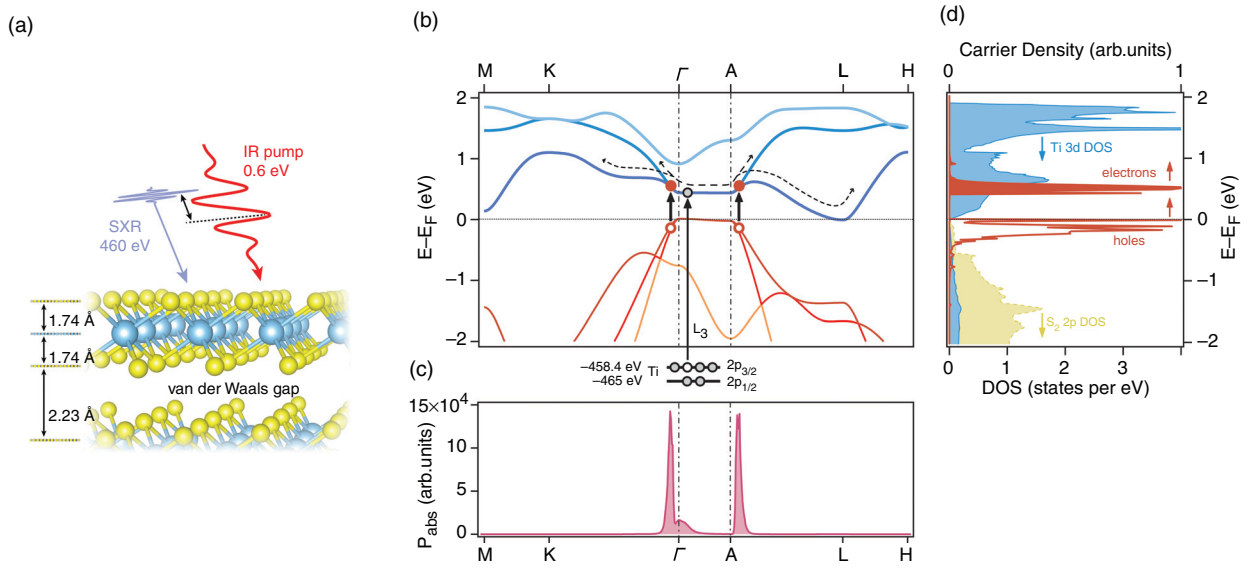

FIG. 2. Soft x-ray absorption spectroscopy in TiS_2. (a) A sub-2-cycle 1.85-μm (0.6 eV) pump pulse stimulates carrier dynamics inside a 150-nm-thin TiS_2 crystal (sketched are two layers), which is probed by a 165-as-duration SXR pulse. (b) DFT calculated band structure showing three valence and conduction bands around the Fermi energy in the first Brillouin zone. Superimposed are single-photon transition pathways between valence and conduction bands from the expected carrier population, shown in (c), for the experimental excitation spectrum. The excitation is localized around the Γ and A valley points. (d) Shows excited carriers depending on energy integrated over momentum space. This corresponds to the electron (red, filled) and hole (red, empty) population, as it would be observed by Pauli blocking in non-momentum resolved XANES, and by assuming the experimental pump spectrum and one-photon transitions. Also shown is the density of states for Ti-3d (blue) and S_2-2p (yellow) orbitals. It can be seen that the majority of carrier density is expected in a narrow energy range centered around 0.55 eV above the Fermi energy.

forces. This weak interlayer bonding results in physical properties that are anisotropic to an extent that the material can be regarded as quasi-two-dimensional solid and thus highly amenable to ion-intercalation in Li-ion batteries.[79] Moreover, the material's band structure changes only marginally when reducing dimensionality from the bulk to the monolayer.[80] These features render TiS_2 of interest as a platform for ultrafast optoelectronic devices and field-effect transistors,[80] for solid-state batteries,[81] and for high-density energy storage.[82] Most notably, we point out that there is a great desire to apply ATAS to the study state-specific carrier dynamics in equally anisotropic systems, e.g., 2D TMDCs, which have garnered significant recent excitement due to the discovery of their unique properties (i.e., Moire excitons,[83–87] charge density waves,[88] superconductivity,[89] valley-selective optical excitation,[90] magnetism,[91] etc.) that are highly tunable with external stimuli and not well understood. Understanding the carrier dynamics in a 3D TMDC like TiS_2 that exhibits a minimal change in band structure with reduced dimensionality will also serve as a control case to provide insight into edges to probe and properties to look for in future studies performed in the 2D limit.

We will show that attosecond-resolution XANES,[57,75,92,93] a variation of ATAS that focuses on the near-edge structure and achieves state-selective interrogation of the 3d orbitals of the transition metal atom Ti. Since XANES relies on dipole transitions from core-states, this translates into accessing the 2p-core to 3d-valence transition in Ti and requiring attosecond pulses at a photon energy of 460 eV. By examining the optoelectronic response under previously unexplored conditions, we show that semi-metals can be a viable material for light-wave electronics in the more technologically relevant case of a weak optical field.

A. Results: Attosecond XANES on TiS_2

Here, we demonstrate a state- and attosecond-resolved investigation of the nonequilibrium dynamics of carriers in the 3d-character conduction band in the presence of an electric control field that is weak enough to be realistically achievable in devices, e.g., with plasmonic nano-focusing,[94,95] in contrast to the strong-field measurements mentioned earlier. Figure 2(b) shows the semi-metallic band structure of bulk TiS_2 calculated from first principles in the density-functional theory framework (DFT); see supplementary material. The angular momentum character of the valence bands originates from mixed sulfur 3p and 3s states. In contrast, the conduction bands are nearly exclusively of Ti 3d character.

The material's optoelectronic response was probed by applying a NIR optical control field at photon energy centered at 0.6 eV. Thus, this optical field could directly bridge the 0.23 eV gap of the valence and conduction bands between the Γ and A points by single-photon excitation while avoiding excitation of high-lying conduction bands excursions beyond the first Brillouin zone. Calculations using the optical spectrum (see supplementary material) show that the excitation is localized around the Γ and A critical points [Fig. 2(c)]. Projecting the momentum-dependent valence excitation onto the transition energy [Fig. 2(d)] indicates energetically narrow contributions to the XANES since the Pauli exclusion principle dictates that fermions cannot transition into already occupied electronic states, an effect often referred to as "Pauli blocking."

The control field consists of a CEP, stable, 1.8-cycle-duration (12 fs FWHM) laser pulse at a center wavelength of 1850 nm, a low-energy replica of the pulse that produced the isolated attosecond SXR

pulse through high harmonic generation. The peak intensity of the control field was 4.1 ± 0.8 10^{11} W cm^{-2}, corresponding to an electric field amplitude of 0.08 V/Å (compared to the 2–2.5 V/Å fields implemented in experiments mentioned in Sec. I B) inside the material and an excitation of 0.03 electrons per unit cell, or a carrier density of 1.94 × 10^{21} cm^{-3}. An essential aspect of resolving in the material response on the scale of the electric field waveform of the control field is, in addition to the SXR pulse attosecond duration, a fast core-hole decay of the material.[96] We estimate a core-hole decay of 3 fs for the Ti 2p states from Ref. 97. The core-hole decay is faster than the cycle period of the control field (6.1 fs at 0.6 eV), consistent with our measurement that shows that the dynamics are indeed resolved on the sub-cycle scale of the optical field.

In the experiment, the SXR attosecond probe interrogated a 150-nm-thick, free-standing, mono-crystalline 1T-TiS_2 sample at 26° incidence of the basal plane normal to sample. A 20-μm-thick Ni pinhole of 100-μm diameter was positioned on top of the TiS_2 sample to define the area of spatial overlap between the attosecond probe and the IR control field. The measurement was taken with a home-built spectrometer consisting of a reflective 2400 lines/mm grating (Hitachi) and a cooled CCD-camera (PIXIS, Princeton Instruments) readout. To state-resolve the dynamics of carriers in the 3d-character conduction band with XANES, we use isolated 165-as-duration SXR[14,18,98] pulses with a bandwidth covering 200 to 550 eV, thus accessing the Ti 2p core states at –458.4 eV ($2p_{3/2}$) and –465.5 eV ($2p_{1/2}$); see Fig. 3. Shown in Fig. 3(b) is the XANES to identify the positions of the Ti L_2 and L_3 absorption edges that arise due to transitions from the $2p_{1/2}$ and $2p_{3/2}$ core states. The static XANES measurement, i.e., un-pumped and non-time-resolved, serves as a reference, and it is in excellent agreement with measurements taken at the ALBA synchrotron light source ALBA (Barcelona) and well-reproduced by theory (see supplementary material).

Figure 3(a) shows the differential absorption spectrum ($\Delta T = T_{pumped} - T_0$) normalized to the unpumped case (T_0), as IR-pump/attosecond-SXR-probe delay. White bars represent data points that were sorted out when post-processing data based on the signal-to-noise ratio. Negative time values correspond to the SXR probe arriving before the IR control field. A positive (red) value reports an increasing SXR transmission due to the material's field-induced excitation, thus an increased carrier population in conduction band states. Immediately apparent in the measurement is a transient signal with a maximum amplitude of 10%, at twice the oscillation frequency of the IR optical field ($2\omega_{IR}$). The signal exhibits oscillations with excursions to both positive (red) and negative (blue) values; see the supplementary material for a Fourier analysis. Figure 3(b) depicts lineouts of the differential absorption [Fig. 3(a)] at different time delays. It establishes that the control-field-induced carrier dynamics occurs at the bottom of the Ti 3d-character conduction band, closest to the Fermi level. Resolved are the transitions to Ti 3d-character states originating from the two spin-orbit split Ti core states $2p_{1/2}$ and $2p_{3/2}$, corresponding to the absorption edges L_2 and L_3. In the following, we restrict our analysis to the L_3 edge to investigate the carriers' dynamics in Ti 3d orbitals, as the signal observed at the L_2 edge may be mixed with transitions from the L_3 to higher-lying conduction band states.

B. State-resolved dynamics

To obtain a detailed physical insight into the underlying carrier dynamics in TiS_2, we turned to theory. We performed a first-principles electron dynamics simulation of the full pump-probe experiment based on real-time time-dependent density functional theory

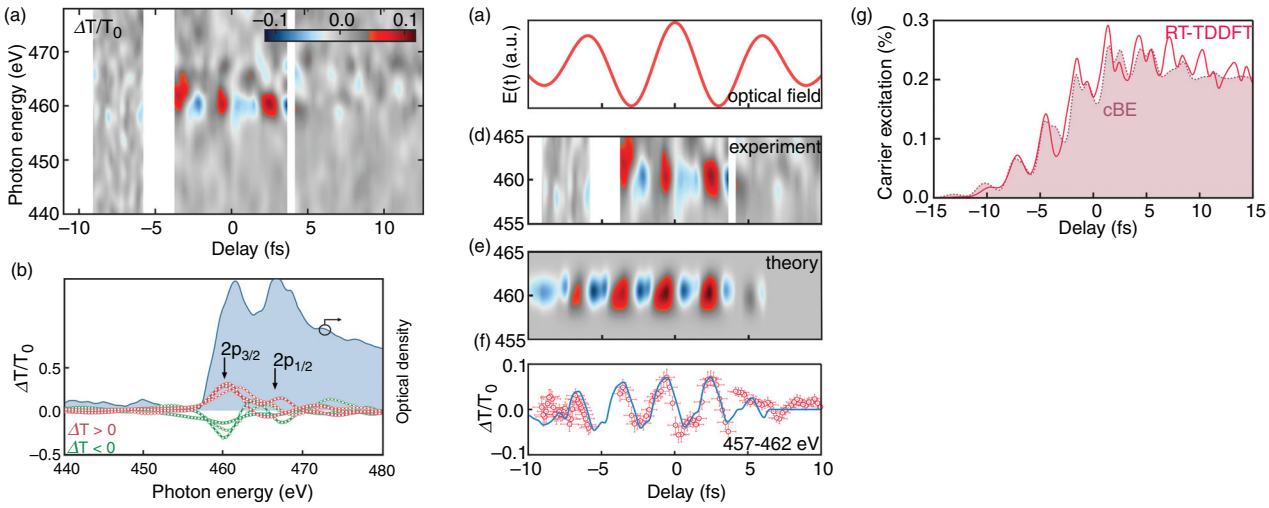

FIG. 3. Time-resolved dynamic in TiS_2. (a) Differential absorption spectrum as a function of pump-probe delay. ΔT is normalized to the un-pumped case T_0 for each time delay. Blanked out areas indicate time ranges without detection. Clearly visible are sub-cycle oscillations of negative and positive differentials with a maximum amplitude of 10%. Time delays were 100 as for negative delays to –5 fs with 6 min integration and 200-as steps with 5 min integration elsewhere. (b) Shows spectral lineouts from (a), taken at the positive and negative extrema (spectral oscillations). The dynamics, red for increased and green for diminished ΔT in relation to the two spin-orbit split states $2p_{3/2}$ and $2p_{1/2}$. (c) Indicates the optical control field. (d) Displays the relevant subsection of (a) for comparison with the cBE calculated differential absorption in (e). (f) Overlays the measurement with the numerical result over the energy region 457–462 eV; error bars originate from the regression algorithm and take the temporal duration (300 as upper limit), temporal walk-off in the material (1.3 fs), and CEP jitter (85 as) into account. (g) Shows the calculated carrier excitation with both models, cBE and RT-TDDFT, of 0.2% corresponding to a carrier density of 1.94 x 10^{21} cm^{-3}.

(RT-TDDFT).[99] In addition to the *ab initio* model, we developed a core-state-resolved Bloch equation model (cBE)[100] to disentangle the various concurrent inter- and intra-band contributions in response to the control field. The cBE model retains the relevant seven bands in three dimensions; it includes the three highest-occupied valence, two lowest-unoccupied conduction band states together with the Ti-2p core states, and bandgap renormalization (further details in supplementary material).

The result of the theory, including the full inter- and intra-band dynamics, is shown in Figs. 3(e), 3(g), and 4. The good qualitative agreement between the measurement [Figs. 3(a) and 3(d)] and calculations [Fig. 3(e)] is depicted in Fig. 3(f), showing the differential absorption integrated over an energy interval of 5 eV where the changes are most prominent (between 457 and 462 eV). Indicated in Fig. 3(c) is the IR control field periodicity, which shows that carriers' response [Figs. 3(d)–3(f)] occurs on the sub-cycle temporal scale with $2\omega_{IR}$ oscillations. We note that the origin of the $2\omega_{IR}$-oscillation has been previously attributed to the DKFE[63,65] and arises due to the ac-Stark effect caused by the external pump field that modulates the electronic wavefunction when transitioning conduction band. From our model, we find that inter-band transitions predominantly occur in the form of one-photon transitions that directly bridge the gap between valence and conduction bands around the Γ and A critical points, as indicated in Fig. 2, and become observable in the transient XANES experiment.

Though beyond the scope of this discussion, we note that time-resolved angle-resolved photoemission spectroscopy (trARPES) can provide complementary information due to the ability to momentum resolve carrier dynamics in the electronic band structure.[101–107] Briefly, trARPES uses an XUV probe pulse with an energy that exceeds the samples' work function (typically 3–6 eV), with higher energies allowing access across the first Brillouin zone. The newly freed electrons are collected by a hemispherical analyzer, whereby the various photoemission angles are tracked to map out the electronic dispersion. Simultaneous measurements, while at first glance appealing due to complementary information, are less straightforward due to trARPES requiring a very narrowband spectrum (ideally 100 meV or less bandwidth) for retaining its energy resolution. At the same time, ATAS's key feature stems from its broadband and ultrafast probing. Besides, trARPES is, like all photoelectron spectroscopies, limited to surface or near-surface states while ATAS can probe the bulk.

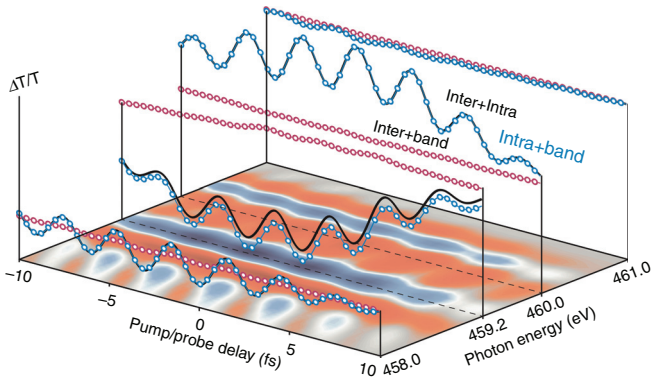

FIG. 4. State-resolved carrier dynamics. Shown is the observed material response as function of pump-probe delay, calculated with the cBE model and including 3 VBs and 4 CBs in full 3D. The surface plot displays the full material response [$\log(\Delta T/T_0)$ where red indicates positive and blue indicates negative values]. The line-outs show the energy-resolved material response (black curve), which is composed of inter- (red) and intra-band (blue) contributions. The dominance of intra-band carriers by one order of magnitude over inter-band carriers is striking; they follow the oscillation of the excitation field and modulate the absorption both positively and negatively.

We used both theoretical models to predict the magnitude of the injection of carriers into the conduction band. Shown in Fig. 3(g) is the result from a projection of the time-dependent wavefunction of the seven-band cBE and the RT-TDDFT model onto the conduction band state. We find excellent agreement among the simulations with an excitation value of 0.2% to the 3d-character conduction band, corresponding to a carrier density of 1.94×10^{21} cm^{-3}.

In general, the transfer of electrons to the conduction band at a specific k-space position results in Pauli blocking and, since the core-level transition (Ti-2p to Ti-3d) accesses conduction band states, this leads to the bleaching of the SXR absorption. Thus, vital is the role of the intra-band motion of carriers. Depending on the mobility, it may diminish (or increase) Pauli blocking at a particular k-space position and manifest as a change of SXR absorption. Therefore, we further investigated the state-resolved dynamics of electrons with a high-resolution cBE calculation. Figure 4 shows the result. Despite the low field strength, we find that immediately visible is the ubiquitous 2ω-oscillation to both positive and negative values, arising from both inter- and intra-band motion. The oscillation to both positive and negative values was never observed before. The signal originated predominantly from intra-band currents, owing to the semi-metal carrier mobility and confirming the absence of Rabi cycling. Overlaid as individual lineouts in Fig. 4 is an energy-resolved decomposition of observed carrier motion into inter- and intra-band contributions. Striking is the dominance of intra-band (blue curves) over inter-band (red curves) carriers and the absorption spectrum's energy-dependent modulation. The absence of apparent chirp is due to the strong and near-instantaneous intra-band carriers' response to the weak driving field. Immediately apparent is the strong modulation of the absorption signatures as a function of time. In the SI, we discuss the origin as Fano-line profile modifications that arise during the optical control field due to the time-modified dipole-phase from excitation into the conduction band.

We further find that the intra-band currents stem from accelerating the carrier population only across 38% of the first Brillouin zone in the presence of the weak electric field. It is worth noting that this relatively small spread, which is driven by intra-band currents, confirms a weak-field regime. This investigation thus contrasts to most strong-field driven solid-state high harmonic experiments, which regularly drive intra-band currents multiple times across the first Brillouin zone.[108]

The intra-band process immediately spreads the conduction band electrons and, thus, reduces the resonant inter-band excitation's energetic localization, reducing the contrast in the experiment for observing carriers following the localized excitation. This result is counter intuitive since one would expect minimal external electric field results in tunneling close to the valence band A and conduction band L points due to the semi-metallic band structure [Fig. 2(b)]. This is a striking finding for optoelectronic applications of semi-metals since it shows, despite gap energies in TiS_2 between 0.23 and 4 eV and a Keldysh parameter of 2.5, tunneling excitation is neither the only nor

the dominant mechanism at play. Instead, the material's response is governed by predominantly one-photon transitions similar to a semiconductor or dielectric material at much higher field strengths.[65,109] A possible reason for this unexpected behavior of the material in a NIR control field is the high density of states between the Γ and A critical points in conjunction with the very high carrier mobility.

Having investigated which contributions are predominant to the carrier dynamics, we turn to exploit the state-selectivity to visualize carriers' spatio-temporal flow. Figure 5 shows the time-dependent charge density oscillations and the density of states (DOS) for two field strengths. We depict the electron density distribution change since it displays the change concerning the ground state (un-pumped case). Red (blue) isosurfaces indicate increasing (decreasing) density. The anisotropic distribution of this charge-density difference reflects the hybridization between Ti-d and S-p states. We found charge depletion along with the chemical bond and an associated increase of electronic density on the Ti state with d-character. These measurement results are consistent with Volkov *et al.*,[66] who demonstrate optically induced electron localization around Ti atoms. The charge redistribution occurs within a femtosecond and over a distance nearing half the distance between Ti and S atoms of 2.4 Å. The charge re-distribution increased in the distance with increasing field amplitude of the NIR laser pulse, thus visualizing the NIR field-driven motion of charged carriers within the unit cell. Interestingly, according to the RT-TDDFT computations at the low field amplitude of 0.08 V/Å, used in this study, the excitation profile of carriers promoted into the conduction band DOS mimics the pump spectrum with transitions originating from valence band states just below the Fermi energy into conduction band states approx. 0.5–1 eV above the Fermi energy; note, this is in excellent agreement with Fig. 2(d). Discernible is also an energy gap between the depopulated valence and populated conduction band states.

The present measurement provides the first unambiguous investigation of the Ti:3d binding orbital, which determines the response of the TMDC to an external light field. Our investigation reveals that localization of electron density occurs around the Ti atoms within a fraction of the optical control field's single-cycle. The change in electronic density is huge for the weak optical excitation field. It modifies the semi-metallic TMDC, leading to strong intra-band currents and behavior like the DKFE, previously only observed in a wide-bandgap system.[63] This raises the interesting question as to whether the DKFE is truly a strong-field effect, and we note that the relevant metric is rather the strength of the control field relative to the size of the bandgap. If the latter is true, semi-metals will be promising candidates for light-wave electronics, requiring much weaker control fields.

III. CONCLUSIONS AND OUTLOOK

We have described the recent developments of attosecond technology and x-ray spectroscopy. We have detailed both how the convergence of methods currently allows researchers to probe the fine structure of an absorption edge in a multi-component material system in real-time. This capability provides the state-resolved dynamics of charge carriers *in situ*. Beyond the field's background, we showcase the state of the art with an attosecond XANES measurement at the Ti $L_{2,3}$ edge at 460 eV of a TMDC quantum material. We described how the core-state-resolved XANES method isolates Ti 3d orbitals' spectral

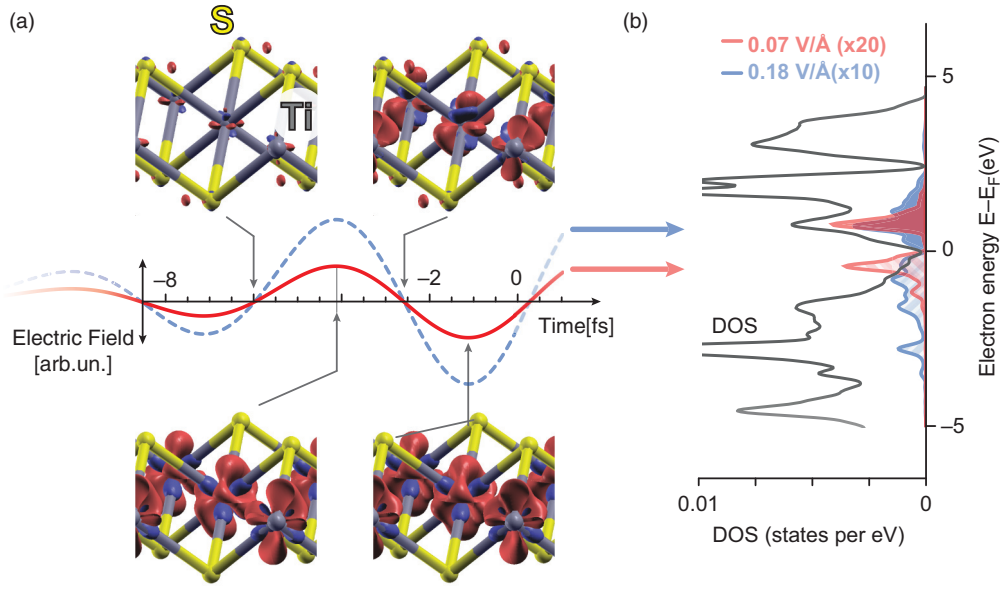

FIG. 5. Spatio-temporal carrier dynamics. (a) At different moments within the electric field oscillation, the difference of electron density is displayed with respect to the ground state (four panels showing the carrier density displacement within the unit cell). Increased density is shown in red and decreasing density in blue. The time-dependent difference shows enhanced localization of population at Ti-d orbitals. These changes occur with a spatial extent up to half the nearest neighbor distance and oscillate predominately with the half-cycle period. (b) Density of states (DOS) and light-induced occupation: RT-TDDFT computations observe the transition from distribution of occupied states within the DOS split in accordance with the pump pulse spectrum for the field amplitude studied in this experiment (occupied DOS in red) toward a more distributed excitation profile extending both into higher and lower energetic intervals of the valence and conduction bands already for a peak field amplitude approximately twice the experimental value (occupied DOS in blue).

contributions, thus accessing the optoelectronic response of the semimetallic TMDC TiS_2 with attosecond temporal resolution and orbital selectivity. The results presented here suggest that TiS_2 is a promising candidate for PHz field-effect devices since very moderate optical fields achieve efficient photo-doping to strikingly high carrier concentrations. This means that weak optical fields can modulate the material response quasi-instantaneously, i.e., without measurable delay, on an optical field's sub-cycle scale. Our investigation of the TMDC TiS_2 provides new insight into the usage of semi-metal TMDCs as building blocks, such as optical field-effect transistors for the next generation of optoelectronic devices' light-wave electronics. While showcasing what is possible with attosecond soft x-ray XANES on the particular example of the TMDC, we stress that such investigations will allow access to the exact interaction of electrons, holes, and lattice modes. This method will provide insight into the entire time-history of charge and lattice dynamics in materials. The prospects are spectacular since the method applies to gases, liquids, solids, and amorphous systems. Monolayer systems such as graphene, BN, or TMDCs may be probed in reflection. In contrast, nanometer-size systems such as composite quantum materials like BN-sandwiched graphene and TMDCs, or adsorbates, can be measured in transmission. We note that an insightful connection between the measured absorption spectrum and the embedded electronic and lattice dynamics is only possible in the simplest of systems without theory. Therefore, new theories are needed to describe the nonequilibrium dynamics of the multi-body state with the pump and probe photons. Presently, such developments are already underway (largely) based on real-time implementations of density functional theory, either in real or reciprocal space. We also expect that XFEL sources will provide attosecond temporal resolution and sufficiently reduced timing jitter soon. XFEL sources will increase present capabilities to the hard x-ray regime. The possibilities are excellent to gain unprecedented and comprehensive insight into the intricate interplay between charge carriers and lattice, which determine the response of materials to an external stimulus. We believe that the described tools will become decisive to move toward an engineered approach to design advanced materials and devices based on exact knowledge of their functionalities. While serendipity has served us surprisingly well, e.g., with the recent discovery of twisttronics with magic-angle graphene, today's societal challenges demand drastically new solutions that are tractable systematically and predictably. The projected increased demand for energy-efficient information processing and storage devices supersedes energy production growth over the next 20 years. With the possibility to scrutinize loss channels in electronic transport and material excitation, we would have a tool to identify possible mitigation strategies to approach the long-sought Landauer limit of information processing devices. We envision studies of charge and lattice dynamics on heterostructures of conventional and quantum materials such as, e.g., Si, Ge, graphene, graphite, BN, TMDCs, and high-Tc superconductors like YBaCuO, TiBaBaCuO, or K_3C_{60}. Based on the exact knowledge of the response of such materials, computer models may be able to predict how combinations of materials can achieve systems in which, e.g., ballistic transport is topologically protected, or in which the valley and spin degrees of freedom are leveraged to store and switch information with THz to PHz speeds. Intimately related with such a goal is the investigation of canonical physics questions, since they have an immediate impact on society. For instance, it is still debated what exactly triggers the superconductive state of a high-Tc superconductor like LaBaCuO, YBaCuO, or, e.g., K_3C_{60}, and contradicting theories exist to describe the mechanism. New insights into Mott physics would be directly relevant for multi-body quantum dynamics and further our understanding of quantum simulators. As such, the application of ATAS toward the study of materials will likely be of great benefit to re-examine long-standing questions of, for example, phase-transitions,[110,111] superconductivity in layered materials,[112] and emergent electronic properties in low-dimensional systems.

SUPPLEMENTARY MATERIAL

See the supplementary material for further experimental details such as the static XANES, calibration measurements at the synchrotron light source ALBA, investigation of the pump absorption and dynamics, the data analysis, and information about the sample growth and preparation. We also include information about the various density-functional theory simulations and the core-resolved Bloch Equation Model.

AUTHORS' CONTRIBUTIONS

J.B. conceived and supervised the project. B.B. and I.L. performed the experiments and analyzed the data. N.D.P. and S.C. contributed to the experimental setup. A.P. performed the SBE calculations, C.C., C.D., M.U., and K.Y. conducted the DFT and TDDFT modeling. E.P. and J.H.M. performed calibration measurements at ALBA. S.M.V. and E.C. grew the samples, T.D. cut the samples. IR absorption measurements were conducted with S.W. M.S., E.B., and M.Z. aided J.B. and B.B. in writing the manuscript.

ACKNOWLEDGMENTS

J.B. and group acknowledge financial support from the European Research Council for ERC Advanced Grant "TRANSFORMER" (788218), ERC Proof of Concept Grant "miniX" (840010), FET-OPEN "PETACom" (829153), FET-OPEN "OPTOlogic" (899794), Laserlab-Europe (EU-H2020 654148), MINECO for Plan Nacional FIS2017-89536-P, AGAUR for 2017 SGR 1639, MINECO for "Severo Ochoa" (SEV-2015-0522), Fundació Cellex Barcelona, CERCA Programme/Generalitat de Catalunya, and the Alexander von Humboldt Foundation for the Friedrich Wilhelm Bessel Prize. A.P. acknowledges Marie Sklodowska-Curie Grant Agreement No. 702565. I.L. acknowledges MINECO for a Juan de la Cierva postdoctoral fellowship, and B.B. acknowledges support by the Severo Ochoa Fellowship program for her PhD fellowship. S.M.V. and E.C. acknowledge funding from the EU (Advanced ERC Grant SPINMOL), the Spanish MINECO (Grant No. MAT2014-56143-R, the Unit of Excellence Maria de Maeztu No. MDM-2015-0538, and the SOMM Alliance). S.M.V thanks the Spanish MINECO for FPU Grant (No. FPU14/04407). M.U. was supported in part by MEXT as a social and scientific priority issue (creation of new functional devices and high-performance materials to support next-generation industries) to be tackled by using post-K computer. M.Z. acknowledges support by the Max Planck Society (Max Planck Research Group) and the Federal Ministry of Education and Research (BMBF) under "Make our Planet Great Again – German Research Initiative" (Grant No. 57427209 "QUESTforENERGY") implemented by DAAD. C.D. and C.C. acknowledge partial support from the German Research

Foundation (DFG) and IRIS Adlershof. We thank Dr. D. Zalvidea, Professor A. Bachthold, Professor J. Garcia de Abajo, and H.-T. Chang for helpful and inspiring discussions, and Professor T. Ra'anan, Professor C. Ropers, and Dr. P. Schmidt for assistance with the sample preparation.

DATA AVAILABILITY

The data that support the findings of this study are available from the corresponding author upon reasonable request.

REFERENCES

[1]R. W. Schoenlein *et al.*, "Generation of femtosecond pulses of synchrotron radiation," Science **287**, 2237–2240 (2000).
[2]G. Ingold *et al.*, "Technical report: FEMTO: A sub-ps tunable hard x-ray undulator source for laser/x-ray pump-probe experiments at the SLS," Synchrotron Radiat. News **20**, 35–39 (2007).
[3]C. Peth, F. Barkusky, and K. Mann, "Near-edge x-ray absorption fine structure measurements using a laboratory-scale XUV source," J. Phys. D. Appl. Phys. **41**, 105202 (2008).
[4]I. Mantouvalou *et al.*, "High average power, highly brilliant laser-produced plasma source for soft x-ray spectroscopy," Rev. Sci. Instrum. **86**, 035116 (2015).
[5]M. Ferray *et al.*, "Multiple-harmonic conversion of 1064 nm radiation in rare gases," J. Phys. B At. Mol. Opt. Phys. **21**, L31–L35 (1988).
[6]A. McPherson *et al.*, "Studies of multiphoton production of vacuum-ultraviolet radiation in the rare gases," J. Opt. Soc. Am. B **4**, 595 (1987).
[7]B. Shan and Z. Chang, "Dramatic extension of the high-order harmonic cutoff by using a long-wavelength driving field," Phys. Rev. A **65**, 011804 (2001).
[8]T. Popmintchev *et al.*, "Bright coherent ultrahigh harmonics in the keV x-ray regime from mid-infrared femtosecond lasers," Science **336**, 1287–1291 (2012).
[9]S. L. Cousin *et al.*, "High-flux table-top soft x-ray source driven by sub-2-cycle, CEP stable, 185-μm 1-kHz pulses for carbon K-edge spectroscopy," Opt. Lett. **39**, 5383 (2014).
[10]F. Silva, S. M. Teichmann, S. L. Cousin, M. Hemmer, and J. Biegert, "Spatiotemporal isolation of attosecond soft X-ray pulses in the water window," Nat. Commun. **6**, 1–6 (2015).
[11]S. L. Cousin *et al.*, "Attosecond streaking in the water window: A new regime of attosecond pulse characterization," Phys. Rev. X **7**, 041030 (2017).
[12]J. Li *et al.*, "53-attosecond X-ray pulses reach the carbon K-edge," Nat. Commun. **8**, 1–5 (2017).
[13]N. Ishii *et al.*, "Carrier-envelope phase-dependent high harmonic generation in the water window using few-cycle infrared pulses," Nat. Commun. **5**, 3331 (2014).
[14]S. M. Teichmann, F. Silva, S. L. Cousin, M. Hemmer, and J. Biegert, "0.5-keV soft x-ray attosecond continua," Nat. Commun. **7**, 1–6 (2016).
[15]A. S. Johnson *et al.*, "High-flux soft x-ray harmonic generation from ionization-shaped few-cycle laser pulses," Sci. Adv. **4**, eaar3761 (2018).
[16]M. Schultze *et al.*, "Attosecond bandgap dynamics in silicon," Science **346**, 1348–1353 (2014).
[17]N. Saito *et al.*, "Real-time observation of electronic, vibrational, and rotational dynamics in nitric oxide with attosecond soft x-ray pulses at 400 eV," Optica **6**, 1542 (2019).
[18]B. Buades *et al.*, "Dispersive soft x-ray absorption fine-structure spectroscopy in graphite with an attosecond pulse," Optica **5**, 502 (2018).
[19]D. Popmintchev *et al.*, "Near- and extended-edge x-ray-absorption fine-structure spectroscopy using ultrafast coherent high-order harmonic supercontinua," Phys. Rev. Lett. **120**, 093002 (2018).
[20]P. Emma *et al.*, "First lasing and operation of an ångstrom-wavelength free-electron laser," Nat. Photonics **4**, 641–647 (2010).
[21]J. Duris *et al.*, "Tunable isolated attosecond x-ray pulses with gigawatt peak power from a free-electron laser," Nat. Photonics **14**, 30–36 (2019).
[22]S. Manzeli, D. Ovchinnikov, D. Pasquier, O. V. Yazyev, and A. Kis, "2D transition metal dichalcogenides," Nat. Rev. Mater. **2**, 1–15 (2017).
[23]K. S. Novoselov, A. Mishchenko, A. Carvalho, and A. H. Castro Neto, "2D materials and van der Waals heterostructures," Science **353**, 461–473 (2016).
[24]S. Thiele, W. Kinberger, R. Granzner, G. Fiori, and F. Schwierz, "The prospects of transition metal dichalcogenides for ultimately scaled CMOS," Solid. State. Electron. **143**, 2–9 (2018).
[25]T. Brabec and F. Krausz, "Intense few-cycle laser fields: Frontiers of nonlinear optics," Rev. Mod. Phys. **72**, 545–591 (2000).
[26]P. B. Corkum, "Plasma perspective on strong field multiphoton ionization," Phys. Rev. Lett. **71**, 1994–1997 (1993).
[27]B. Shan and Z. Chang, "Dramatic extension of the high-order harmonic cutoff by using a long-wavelength driving field," Phys. Rev. A **65**, 011404 (2001).
[28]M. Krebs *et al.*, "High repetition rate few-cycle OPCPA for generation of isolated attosecond pulses," High Intensity Lasers High F. Phenomena, HILAS **2012**, 29–31.
[29]U. Elu *et al.*, "High average power and single-cycle pulses from a mid-IR optical parametric chirped pulse amplifier," Optica **4**, 1024 (2017).
[30]K. Hong *et al.*, "Chirped-pulse amplifier and high-flux soft x-ray high-harmonic generation," Opt. Lett. **39**, 3145–3148 (2014).
[31]G. Andriukaitis *et al.*, "90 GW peak power few-cycle mid-infrared pulses from an optical parametric amplifier," Opt. Lett. **36**, 2755 (2011).
[32]V. Cardin *et al.*, "Self-channelled high harmonic generation of water window soft x-rays," J. Phys. B **51**, 1–10 (2018).
[33]A. D. Shiner *et al.*, "Wavelength scaling of high harmonic generation efficiency," Phys. Rev. Lett. **103**, 073902 (2009).
[34]J. Tate *et al.*, "Scaling of wave-packet dynamics in an intense midinfrared field," Phys. Rev. Lett. **98**, 013901 (2007).
[35]D. R. Austin and J. Biegert, "Strong-field approximation for the wavelength scaling of high-harmonic generation," Phys. Rev. A **86**, 023813 (2012).
[36]M.-C. Chen *et al.*, "Generation of bright isolated attosecond soft x-ray pulses driven by multicycle midinfrared lasers," Proc. Natl. Acad. Sci. **111**, E2361–E2367 (2014).
[37]H. Xiong *et al.*, "Generation of a coherent x ray in the water window region at 1 kHz repetition rate using a mid-infrared pump source," Opt. Lett. **34**, 1747 (2009).
[38]C. Ding *et al.*, "High flux coherent super-continuum soft x-ray source driven by a single-stage, 10 mJ, Ti:Sapphire amplifier-pumped OPA," Opt. Express **22**, 6194 (2014).
[39]Y. Fu *et al.*, "High efficiency ultrafast water-window harmonic generation for single-shot soft X-ray spectroscopy," Commun. Phys. **3**, 92 (2020).
[40]C. Vozzi *et al.*, "Millijoule-level phase-stabilized few-optical-cycle infrared parametric source," Opt. Lett. **32**, 2957 (2007).
[41]B. E. Schmidt *et al.*, "Compression of 1.8 μm laser pulses to sub two optical cycles with bulk material," Appl. Phys. Lett. **96**, 121109 (2010).
[42]Y. Deng *et al.*, "Carrier-envelope-phase-stable, 12 mJ, 15 cycle laser pulses at 21 μm," Opt. Lett. **37**, 4973 (2012).
[43]T. Gaumnitz *et al.*, "Streaking of 43-attosecond soft-x-ray pulses generated by a passively CEP-stable mid-infrared driver," Opt. Express **25**, 27506 (2017).
[44]S. R. Leone *et al.*, "What will it take to observe processes in 'real time'?," Nat. Photonics **8**, 162–166 (2014).
[45]X. Ren *et al.*, "Attosecond light sources in the water window," J. Opt. **20**, 023001 (2018).
[46]Y. Cao *et al.*, "Unconventional superconductivity in magic-angle graphene superlattices," Nature **556**, 43–50 (2018).
[47]M. Yankowitz *et al.*, "Tuning superconductivity in twisted bilayer graphene," Science **363**, 1059–1064 (2019).
[48]X. Lu *et al.*, "Superconductors, orbital magnets, and correlated states in magic angle bilayer graphene," Nature **574**, 653–657 (2019).
[49]C. Proust and L. Taillefer, "The remarkable underlying ground states of cuprate superconductors," Annu. Rev. Condens. Matter Phys. **10**, 409–429 (2019).
[50]A. E. Baumann, D. A. Burns, B. Liu, and V. S. Thoi, "Metal-organic framework functionalization and design strategies for advanced electrochemical energy storage devices," Commun. Chem. **2**, 1–14 (2019).
[51]Q. Wang and D. Astruc, "state of the art and prospects in metal–organic framework (MOF)-based and MOF-derived nanocatalysis," Chem. Rev. **120**, 1438–1511 (2020).

[52]D. J. Rizzo *et al.*, "Topological band engineering of graphene nanoribbons," Nature **560**, 204–208 (2018).
[53]P. Yang, "The chemistry and physics of nanowires," MRS Bull. **30**, 85–91 (2005).
[54]R. Schirhagl, K. Chang, M. Loretz, and C. L. Degen, "Nitrogen-vacancy centers in diamond: Nanoscale sensors for physics and biology," Annu. Rev. Phys. Chem. **65**, 83–105 (2014).
[55]M. W. Doherty *et al.*, "The nitrogen-vacancy colour centre in diamond," Phys. Rep. **528**, 1–45 (2013).
[56]X. Liu and M. C. Hersam, "2D materials for quantum information science," Nat. Rev. Mater. **4**, 669–684 (2019).
[57]A. Bianconi, "Surface x-ray absorption spectroscopy: Surface EXAFS and surface XANES," Appl. Surf. Sci. **6**, 392–418 (1980).
[58]P. M. Kraus, M. Zürch, S. K. Cushing, D. M. Neumark, and S. R. Leone, "The ultrafast x-ray spectroscopic revolution in chemical dynamics," Nat. Rev. Chem. **2**, 82–94 (2018).
[59]R. Geneaux, H. J. B. Marroux, A. Guggenmos, D. M. Neumark, and S. R. Leone, "Transient absorption spectroscopy using high harmonic generation: A review of ultrafast X-ray dynamics in molecules and solids," Philos. Trans. R. Soc. A Math. Phys. Eng. Sci. **377**, 1–27 (2019).
[60]M. Schultze *et al.*, "Controlling dielectrics with the electric field of light," Nature **493**, 75–78 (2013).
[61]H. Mashiko, K. Oguri, T. Yamaguchi, A. Suda, and H. Gotoh, "Petahertz optical drive with wide-bandgap semiconductor," Nat. Phys. **12**, 741–745 (2016).
[62]H. Mashiko *et al.*, "Multi-petahertz electron interference in Cr:Al_2O_3 solid-state material," Nat. Commun. **9**, 1468 (2018).
[63]M. Lucchini *et al.*, "Attosecond dynamical Franz-Keldysh effect in polycrystalline diamond," Science **353**, 916–919 (2016).
[64]M. Lucchini *et al.*, "Attosecond timing of the dynamical Franz–Keldysh effect," J. Phys. Photonics **2**, 1–7 (2020).
[65]F. Schlaepfer *et al.*, "Attosecond optical-field-enhanced carrier injection into the GaAs conduction band," Nat. Phys. **14**, 560–564 (2018).
[66]M. Volkov *et al.*, "Attosecond screening dynamics mediated by electron localization in transition metals," Nat. Phys. **15**, 1145–1149 (2019).
[67]A. Starace, "Photoionization of atoms," in *Springer Handbook of Atomic, Molecular, and Optical Physics* (Springer, New York, 2006), 379–390.
[68]F. de Groot, "Multiplet effects in x-ray spectroscopy," Coord. Chem. Rev. **249**, 31–63 (2005).
[69]C. J. Milne, T. J. Penfold, and M. Chergui, "Recent experimental and theoretical developments in time-resolved x-ray spectroscopies," Coord. Chem. Rev. **277**, 44–68 (2014).
[70]M. C. Chen *et al.*, "Bright, coherent, ultrafast soft x-ray harmonics spanning the water window from a table-top light source," Phys. Rev. Lett. **105**, 173901 (2010).
[71]I. L. Markov, "Limits on fundamental limits to computation," Nature **512**, 147–154 (2014).
[72]J. R. Powell, "The quantum limit to Moore's law," Proc. IEEE **96**, 1247–1248 (2008).
[73]R. Lv *et al.*, "Transition metal dichalcogenides and beyond: Synthesis, properties, and applications of single- and few-layer nanosheets," Acc. Chem. Res. **48**, 56–64 (2015).
[74]S. Ahmed and J. Yi, "Two-dimensional transition metal dichalcogenides and their charge carrier mobilities in field-effect transistors," Nano-Micro Lett. **9**, 50 (2017).
[75]J. Stöhr, *NEXAFS Spectroscopy* (Springer, Berlin Heidelberg, 1992), Vol. 25.
[76]F. de Groot and A. Kotani, *Core Level Spectroscopy of Solids* (CRC Press, 2008).
[77]A. Michette, "Introduction to XAFS: A practical guide to x-ray absorption fine structure spectroscopy, by Grant Bunker," Contemp. Phys. **52**, 623–623 (2011).
[78]A. H. Reshak, I. V. Kityk, and S. Auluck, "Electronic structure and optical properties of 1T-TiS_2 and lithium intercalated 1T-TiS2 for lithium batteries," J. Chem. Phys. **129**, 074706 (2008).
[79]S. Sharma *et al.*, "Electronic structure of 1T-TiS_2," Phys. Rev. B **59**, 14833–14836 (1999).
[80]C. S. Cucinotta *et al.*, "Electronic properties and chemical reactivity of TiS_2 nanoflakes," J. Phys. Chem. C **119**, 15707–15715 (2015).
[81]M. S. Whittingham, "Lithium batteries and cathode materials," Chem. Rev. **104**, 4271–4301 (2004).
[82]A. H. Reshak, "Copper-intercalated TiS_2: Electrode materials for rechargeable batteries as future power resources," J. Phys. Chem. A **113**, 1635–1645 (2009).
[83]Y. Shimazaki *et al.*, "Strongly correlated electrons and hybrid excitons in a moiré heterostructure," Nature **580**, 472–477 (2020).
[84]B. Urbaszek and A. Srivastava, "Materials in flatland twist and shine," Nature **567**, 39–40 (2019).
[85]K. L. Seyler *et al.*, "Signatures of moiré-trapped valley excitons in $MoSe_2$/WSe_2 heterobilayers," Nature **567**, 66–70 (2019).
[86]H. Baek *et al.*, "Highly tunable quantum light from moiré trapped excitons," Sci. Adv. **6**(37), eaba8526 (2020).
[87]C. Jin *et al.*, "Observation of moiré excitons in WSe_2/WS_2 heterostructure superlattices," Nature **567**, 76–80 (2019).
[88]A. W. Tsen *et al.*, "Structure and control of charge density waves in two-dimensional 1T-TaS_2," Proc. Natl. Acad. Sci. **112**, 15054–15059 (2015).
[89]E. Navarro-Moratalla *et al.*, "Enhanced superconductivity in atomically thin TaS_2," Nat. Commun. **7**, 1–7 (2016).
[90]T. Cao *et al.*, "Valley-selective circular dichroism of monolayer molybdenum disulphide," Nat. Commun. **3**, 1–9 (2012).
[91]M. Gibertini, M. Koperski, A. F. Morpurgo, and K. S. Novoselov, "Magnetic 2D materials and heterostructures," Nat. Nanotechnol. **14**, 408–419 (2019).
[92]R. Stumm von Bordwehr, "A history of x-ray absorption fine structure," Ann. Phys. **14**, 377–465 (1989).
[93]R. Jenkins, R. W. Gould, and D. Gedcke, *Quantitative X-Ray Spectrometry* (Marcel Dekker, New York, 1981).
[94]M. Sivis *et al.*, "Tailored semiconductors for high-harmonic optoelectronics," Science **357**, 303–306 (2017).
[95]D. A. Iranzo *et al.*, "Probing the ultimate plasmon confinement limits with a van der Waals heterostructure," Science **360**, 291–295 (2018).
[96]A. Moulet, J. B. Bertrand, T. Klostermann, A. Guggenmos, and N. Karpowicz, "Soft x-ray excitonics," Science **357**, 1134–1138 (2017).
[97]M. O. Krause, "Atomic radiative and radiationless yields for K and L shells," J. Phys. Chem. Ref. Data **8**, 307–327 (1979).
[98]X. Zhao *et al.*, "Metrology of time-domain soft x-ray attosecond pulses and reevaluation of pulse durations of three recent experiments," Phys. Rev. Appl. **13**, 1 (2020).
[99]K. Yabana, T. Sugiyama, Y. Shinohara, T. Otobe, and G. F. Bertsch, "Time-dependent density functional theory for strong electromagnetic fields in crystalline solids," Phys. Rev. B **85**, 045134 (2012).
[100]A. Picón, L. Plaja, and J. Biegert, "Attosecond x-ray transient absorption in condensed-matter: A core-state-resolved Bloch model," New J. Phys. **21**, 043029 (2019).
[101]E. J. Sie, T. Rohwer, C. Lee, and N. Gedik, "Time-resolved XUV ARPES with tunable 24–33 eV laser pulses at 30 meV resolution," Nat. Commun. **10**, 1–11 (2019).
[102]Y. H. Wang *et al.*, "Observation of a warped helical spin texture in Bi_2 Se_3 from circular dichroism angle-resolved photoemission spectroscopy," Phys. Rev. Lett. **107**, 207602 (2011).
[103]C. L. Smallwood *et al.*, "Tracking Cooper pairs in a cuprate superconductor by ultrafast angle-resolved photoemission," Science **336**, 1137–1139 (2012).
[104]F. Schmitt *et al.*, "Transient electronic structure and melting of a charge density wave in $TbTe_3$," Science **321**, 1649–1652 (2008).
[105]L. Perfetti *et al.*, "Time evolution of the electronic structure of 1*T*–TaS_2 through the insulator-metal transition," Phys. Rev. Lett. **97**, 067402 (2006).
[106]A. Damascelli, Z. Hussain, and Z. X. Shen, "Angle-resolved photoemission studies of the cuprate superconductors," Rev. Mod. Phys. **75**, 473–541 (2003).
[107]A. Gauthier *et al.*, "Tuning time and energy resolution in time-resolved photoemission spectroscopy with nonlinear crystals," J. Appl. Phys. **128**, 093101 (2020).

[108]G. Ndabashimiye *et al.*, "Solid-state harmonics beyond the atomic limit," Nature **534**, 520–523 (2016).
[109]C. R. McDonald, G. Vampa, P. B. Corkum, and T. Brabec, "Intense-laser solid state physics: Unraveling the difference between semiconductors and dielectrics," Phys. Rev. Lett. **118**, 173601 (2017).
[110]A. Cavalleri *et al.*, "Band-selective measurements of electron dynamics in VO_2 using femtosecond near-edge X-ray absorption," Phys. Rev. Lett. **95**, 067405 (2005).
[111]M. Rini *et al.*, "Transient electronic structure of the photoinduced phase of $Pr_{0.7}Ca_{0.3}MnO_3$ probed with soft x-ray pulses," Phys. Rev. B **80**, 1–5 (2009).
[112]Y. Maeno *et al.*, "Superconductivity in a layered perovskite without copper," Nature **372**, 532–534 (1994).
[113]H. Timmers, M. Sabbar, J. Hellwagner, Y. Kobayashi, D. M. Neumark, and S. R. Leone, Optica **3**, 707 (2016).